Single-Frequency Violet and Blue Laser Emission from AlGaInN Photonic Integrated Circuit Chips

THOMAS WUNDERER[1,*,+], ANAT SIDDHARTH[2,+], NOBLE M. JOHNSON[1], CHRISTOPHER L. CHUA [1], MARK TEEPE[1], ZHIHONG YANG[1], MAX BATRES[1], PATRICK MAEDA[1], GRIGORII LIKHACHEV[2], AND TOBIAS J. KIPPENBERG[2]

[1] *Hardware Research and Technology Laboratory, Palo Alto Research Center (PARC), Palo Alto, 94304 CA, USA*
[2] *Laboratory of Photonics and Quantum Measurements, Swiss Federal Institute of Technology Lausanne (EPFL), CH-1015 Lausanne, Switzerland*
[+] *T.W. and A.S. contributed equally to this work*
[*] *Corresponding author: wunderer@parc.com*

Compiled January 31, 2023

Chip-based, single-frequency and low phase-noise integrated photonic laser diodes emitting in the violet (412 nm) and blue (461 nm) regime are demonstrated. The GaN-based edge-emitting laser diodes were coupled to high-Q on-chip micro-resonators for optical feedback and mode selection resulting in laser self-injection locking with narrow emission linewidth. Multiple group III-nitride (III-N) based photonic integrated circuit chips with different waveguide designs including single-crystalline AlN, AlGaN, and GaN were developed and characterized. Single-frequency laser operation was demonstrated for all studied waveguide core materials. The best side-mode suppression ratio was determined to be $\sim$ 36 dB at 412 nm with a single-frequency laser emission linewidth of only about 3.8 MHz at 461 nm. The performance metrics of this novel type of laser suggest potential implementation in next generation, portable quantum systems.

http://dx.doi.org/10.1364/ao.XX.XXXXXX

1. INTRODUCTION

Compact, high-performance laser sources that operate in the visible to the ultraviolet spectral regime will be essential to realize field-deployable optical quantum systems. Applications for such systems range from quantum metrology, and sensing based on laser-cooled neutral atoms and ions to next-generation optical atomic clocks, optical quantum computing, interferometric bio-photonics, and visible spectroscopy [1–4]. Specifically, laser Doppler-cooling of many relevant atoms and ions require precision sources at target wavelength in the UV and visible regime (e.g., Yb+ (369 nm), Ca+ (397 nm), Yb (399 nm), Sr+ (421 nm), and Sr (461 nm) [5–7]. Similarly, barium ions are interesting for quantum networking with relevant transitions at 455 and 493 nm. In addition, compact, narrow-linewidth blue sources would enable underwater laser range-finding (i.e., LiDAR) and communications [8], and PIC chips designed for beam steering via optical phased arrays have been proposed for emerging applications such as augmented and virtual reality displays. Today, however, most of the demanding laser specifications are only met using larger-sized, extended-cavity laser systems [9], limiting the addressable application space.

2. HYBRID PHOTONIC INTEGRATED LASER

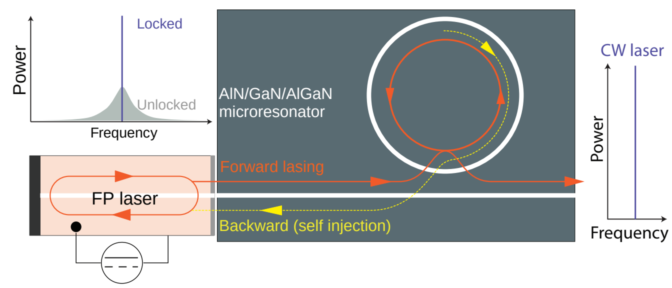

Fig. 1. Schematic of laser concept. A GaN-based Fabry-Pérot laser diode is butt-coupled to a crystalline III-N PIC chip with either AlN, AlGaN, or GaN waveguide core. When light from the laser diode is properly coupled into the micro-resonator via evanescent coupling from the bus waveguide backwards reflected photons can be amplified in the gain region resulting in laser self-injection locking and single-frequency operation. The reduction of the laser emission linewidth is proportional to the quality factor Q of the micro-resonator.

Here, we describe a compact, chip-based laser concept that offers single-frequency, low phase-noise laser radiation with a vastly reduced form factor [10–12]. Figure 1 shows a schematic of the hybrid-integrated laser concept. A GaN-based Fabry–Pérot laser diode chip is butt-coupled to a III-N PIC chip with an integrated high-Q micro-resonator for optical feedback and mode-selection. A fraction of the photons that are evanescently coupled [13] between the bus waveguide and the micro-resonator are backscattered into the gain region of the LD, where they are

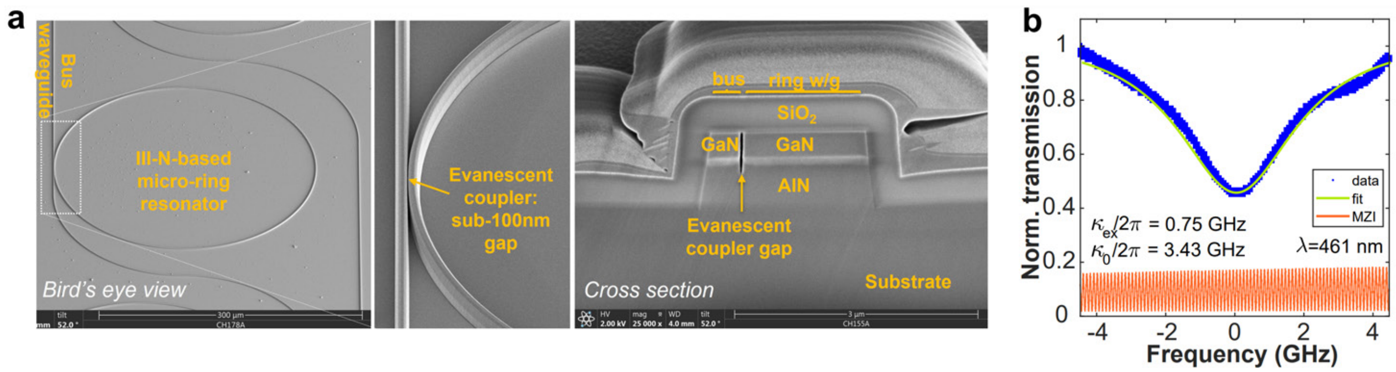

Fig. 2. (a) SEM image of III-N-based PIC chip with GaN waveguide core. The SEM images show a bird's eye view of the evanescently coupled micro-ring resonator (left), a zoom-in view of the coupler area (middle), and a cross section view of the evanescent coupler region at the narrowest gap position. In this example, GaN is the waveguide core material, whereas AlN acts as bottom cladding and SiO_2 as top and side cladding. (b) Cavity transmission of a crystalline III-N PIC chip with AlN waveguide core, exhibiting intrinsic quality factor of 1.9×10^5.

amplified, resulting in laser self-injection locking, and single-frequency laser operation [14]. The minimum achievable laser emission linewidth is proportional to the quality factor Q of the micro-resonator.

A. Laser diode fabrication and performance

The laser diodes were custom designed and fabricated from AlGaInN alloys for operation in the near UV spectral band. The heteroepitaxial structure was grown on bulk single-crystal GaN substrates of low dislocation density by Metal-Organic Vapor Phase Epitaxy (MOVPE). The epitaxial growth process was optimized by balancing the optical and electronic performance of the device to achieve high optical gain and low absorption losses within the laser heterostructure. The active zone of the laser diode consisted of multiple InGaN quantum wells that are electrically pumped in a vertical pn-junction configuration. The material and structural parameters were adjusted for laser emission near 410 nm. In this edge-emitter configuration, optical confinement of the transverse mode was realized in the vertical heterostructure layer stack with the active Multi-Quantum Well (MQW) zone embedded in the (Al)Ga(In)N waveguide and cladding layers of varying Al-compositions. Lateral mode confinement was achieved via dry etching a narrow ridge into the p-layer of the heterostructure and creation of high optical gain in the QWs directly below the etched ridge. Lateral current confinement and the creation of localized gain were accomplished by ensuring electrical current injection exclusively through a via in the electrical passivation layer above the laser ridge. The width of the laser ridge was nominally 1.5 μm and the depth of the etched ridge was optimized for laser operation in a single lateral mode. Laser mirror facets were realized via cleaving along the crystallographic m-plane of the III-N crystal. The length of the laser resonator cavity was nominally 1 mm. Select optical mirror coatings were applied to the front and rear facets to optimize the laser emission characteristics. For continuous wave (CW) operation, individual laser diodes (LD) were mounted epi-side up onto thermal heat-spreader submounts, with wire bonding to n- and p-contact pads. The LD-heat spreader sub-mount ensemble was then mounted in a standard TO-5 header. Precision mounting and alignment in the experimental test system enabled full access to the laser facet for optimal butt-coupling of the LD to the PIC chip. The laser diodes displayed characteristic lasing thresholds near 70 mA and produced more than 100 mW of continuous-wave optical output power at a wavelength of 410 nm.

B. III-N PIC chip fabrication and characterization

In this study, we describe Photonic Integrated Circuit components and sub-systems that are compatible for operation at UV to IR wavelengths. Specifically, (ultra) wide band gap (UWBG), single-crystalline semiconductor materials were implemented as the waveguide core material of the PIC components. As the achievable laser linewidth and quality factor Q of the on-chip micro-resonators strongly depend on absorption and scatter losses, minimizing these becomes essential. This is why we followed fabrication principles that are similar to the laser diode processes described above. The PIC chips were realized using epitaxially grown, single-crystalline group III-nitride (III-N) films. The semiconductor films were grown by MOVPE, essentially using the same fabrication tools as for the active laser diode components. Three different sample types with different waveguide core materials were investigated. PIC chips with AlN, AlGaN and GaN core waveguide designs were developed and characterized. Sapphire (Al_2O_3) was used as the substrate for all samples. In the case of the AlN core the sapphire substrate also acted as bottom cladding, whereas for the other two samples AlN fullfilled this function.

Lateral PIC component definition was realized via high-resolution e-beam lithography and pattern transfer using a subtractive etch process. The process was optimized to allow smooth waveguide side walls, steep etch angles, and high aspect ratios (e.g., etch depth of > 1 μm, with gap sizes < 100 nm). After the etch process was completed SiO_2 was deposited onto the patterned components, acting as top and side wall cladding of the waveguides. As an example, Figure 2 shows SEM images of the PIC chip with GaN waveguide core. Bird's eye views and the cross section image were taken at the smallest gap position between the bus waveguide and micro-resonator.

To evaluate the quality of the produced III-N PIC chips, and in particular the one of the micro-resonators, cavity resonance linewidth measurements were performed using a tunable external-cavity diode laser at 461 nm. For the PIC sample with GaN core waveguide a loaded cavity linewidth $\kappa/2\pi = 6.03$ GHz and an intrinsic linewidth $\kappa_0/2\pi = 3.89$ GHz were determined,

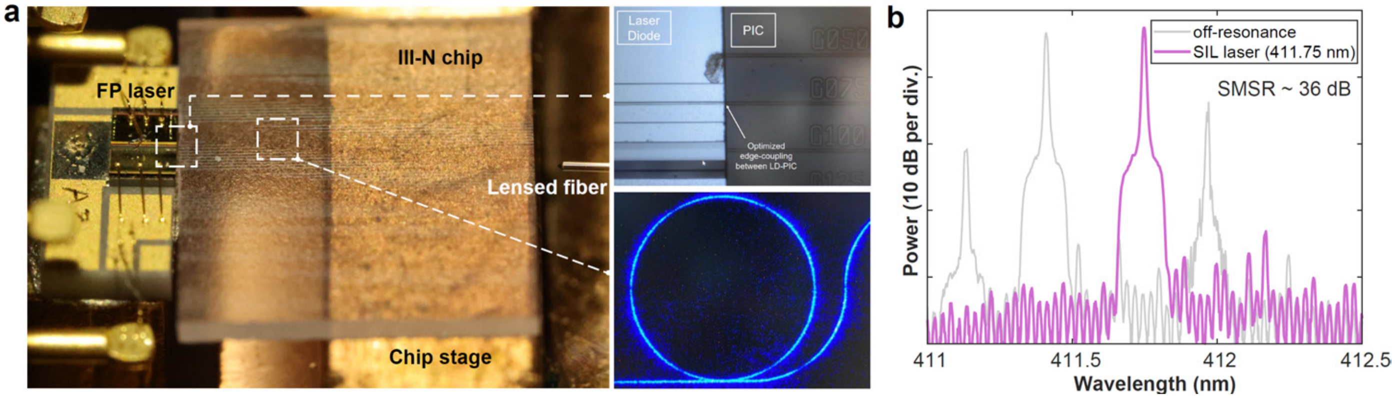

Fig. 3. III-N hybrid integrated laser at 412 nm. (a) Photograph of the hybrid integrated laser placed on the experimental setup. The insets show edge-coupling between GaN LD and III-N PIC chip and Photo of III-N micro-resonator with coupled blue light. (b) Single frequency laser emission at 412 nm with 36 dB side-mode suppression ratio (SMSRs).

corresponding to an intrinsic quality factor of $\sim 0.17 \times 10^6$. The sample with pure AlN core performed slightly better with $\kappa/2\pi$ = 4.17 GHz and $\kappa_0/2\pi$ = 3.43 GHz, resulting in an estimated intrinsic quality factor of $\sim 0.19 \times 10^6$. The AlGaN sample showed a very comparable value with $\sim 0.17 \times 10^6$. These numbers compare quite favorably with other PIC chips designed for operation at UV-blue wavelengths, especially to those with high optical confinement [15–19].

C. Laser self-injection locking and single-frequency operation

Next, the individually optimized LDs and PIC chips were carefully aligned for optimal edge-coupling between the LD mirror facet and the PIC chip input coupler facet (Fig. 3(a)). Both the LD and the PIC chip were thermally stabilized avoiding any uncontrolled thermal drift. Laser self-injection locking was attained when the frequency of the laser emission overlapped with a high-Q resonance of the III-N micro-ring resonator and optical feedback phase conditions were met by optimizing the distance between LD and PIC. When tuning the electrical current of the laser diode and, thus, sweeping the relative frequency between the laser and the micro-resonator modes self-injection locking can be obtained for a given parameter set. As long as the laser operates within the locking range no mode hoping is observed and stable single-frequency operation can be accomplished. The measured optical output power from the single-frequency laser with AlN PIC, collected via a lensed fiber at the PIC output port, exceeded 0.5 mW at 412 nm. The side-mode suppression ratio (SMSR) was as high as 36 dB (Fig. 3(b)). The tested PIC lasers with AlGaN and GaN core showed a lower output power, which might be caused by inferior coupling to the waveguides and to a lesser degree from increased absorption or scatter losses.

D. Laser frequency noise measurements

Figure 4(a) illustrates the experimental approach for determining the frequency noise of the laser. The laser frequency noise was measured by performing heterodyne beat-note spectroscopy with a tunable external cavity diode laser (Toptica DLC DL pro HP) at a central wavelength of 461 nm as the reference. The electrical output of the photodiode was fed to a spectrum analyzer (Rhode and Schwarz FSW43). Figure 4(b) shows the heterodyne beat-note of the self-injection locked laser with the reference laser. The spectrum was fitted with the Voigt profile, which provides information about the Lorentzian and Gaussian contribution to the frequency noise. The Lorentzian part is linked to the white noise and defines the intrinsic linewidth, whereas the Gaussian part corresponds to the 1/f (flicker) and technical noise of the laser. From fitting, we extracted a Lorentzian linewidth of 3.77 MHz and Gaussian FWHM of 3.92 MHz. Figure 4(c) shows the frequency noise spectra of the free-running Fabry–Pérot laser and the self-injection locked laser. The frequency noise of the laser is determined via Welch's method from a time sampling trace of the in-phase and quadrature components of the beat-note. The single sided phase noise power spectral density (PSD) $S_\phi(f)$ was converted to frequency noise $S_\nu(f)$ according to $S_\nu(f) = f^2 \cdot S_\phi(f)$. The self-injection locked laser optical spectrum is shown in Figure 4(d) indicating laser emission wavelength at 462.1 nm with side-mode suppression ratio of 29 dB. We also used the beta-line to quantify the linewidth of the self-injection locked laser by integrating the PSD from the intersection of the frequency noise curve with the beta-line $S_\nu(f) = 8\ln(2)f/ß^2$ down to the integration time of the measurement. The integrated frequency noise A is used to evaluate the full-width half-maximum measure of the linewidth using $\mathrm{FWHM} = \sqrt{8 \cdot \ln(2) \cdot \mathrm{A}}$ [20]. We estimate the FWHM to 3.94 MHz at 10 μs integration time, being in very good agreement with the Voigt fit.

3. SUMMARY

In summary, we have demonstrated all III-nitride single-frequency hybrid photonic integrated lasers operating at violet (412 nm) and blue (462 nm) wavelengths. Custom AlGaInN-based laser gain elements were butt-coupled to III-N photonic integrated micro-resonators featuring high-Q and providing optical feedback and mode selection for laser self-injection locking. The intrinsic quality factor of the III-N micro-resonators were as high as 0.2×10^6 at a wavelength of 461 nm. The high-quality factor of our platform ensures single longitudinal mode lasing at blue to violet wavelengths with laser linewidths as low as 3.8 MHz, a value traditionally only achieved with large-sized external cavity diode lasers. Further improvements in noise performance can be expected with additional advances in the chip design and process optimization. We trust that by optimizing both the coupling between the laser-to-chip and chip-to-fiber and modest improvements in the device quality factor, multi-mW output powers and sub-100 kHz optical linewidths in the near-ultraviolet and UV-A region are feasible, making our systems promising candidates for compact laser implementations

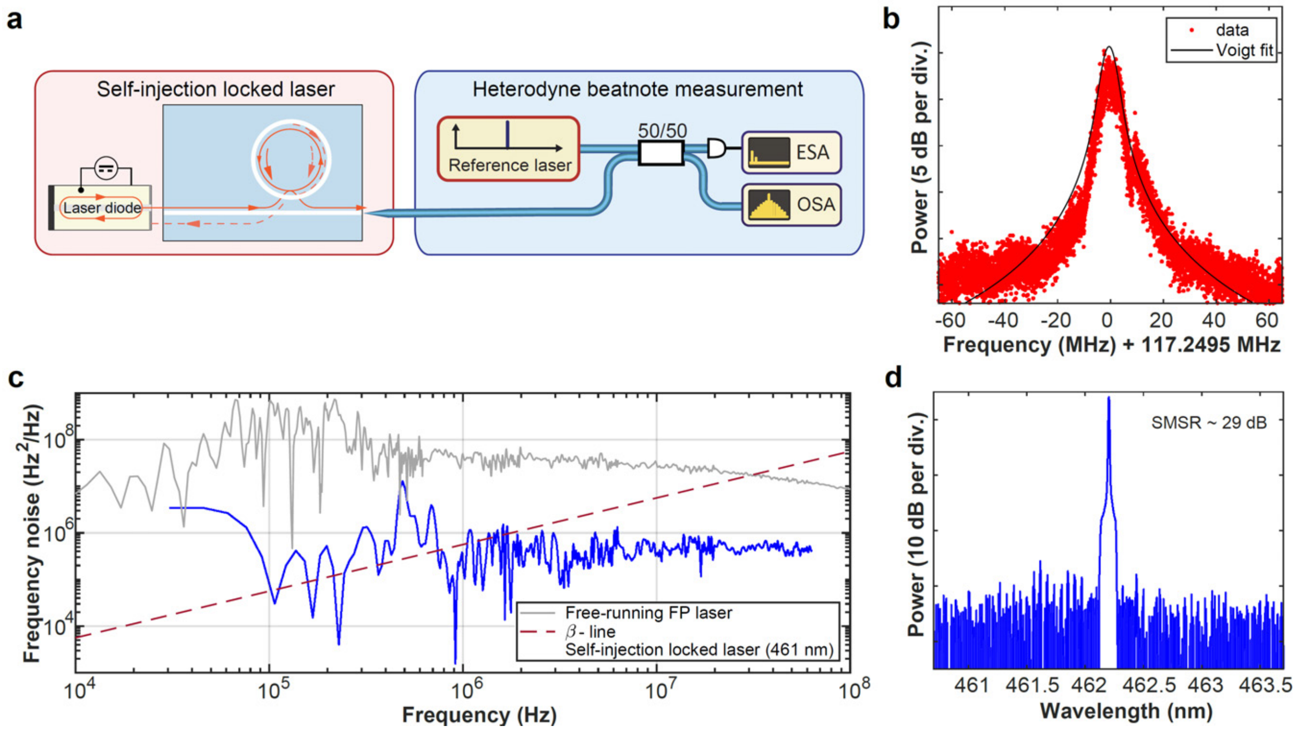

Fig. 4. III-N hybrid integrated laser performance characterization at 461 nm. (a) Experimental scheme of laser frequency noise measurement using heterodyne beat with the reference laser (Toptica DL Pro) at 461 nm. (b) Heterodyne beat signal between the injection-locked laser and the reference laser. The measured beat signal is fitted with Voigt profile with Lorentzian FWHM ∼3.76 MHz and Gaussian FWHM ∼3.92 MHz. (c) Single sideband frequency noise PSD of the hybrid integrated laser upon self-injection locking to microresonator with FSR 107.08 GHz. The grey line shows the frequency noise of a free-running Fabry-Pérot laser diode. β-line is shown as a reference (dashed line). (d) Optical spectrum of the self-injection locked Fabry-Pérot laser showing emission at 462.1 nm with 29 dB side-mode suppression ratio (SMSRs).

in next generation quantum systems, e.g., for Sr+, Ca+, and Yb+ atomic clocks.

Funding. This work was sponsored by the Army Research Laboratory under Agreement No. W911NF-19-2-0345. A.S. acknowledges support from the European Space Technology Centre with ESA Contract No. 4000135357/21/NL/GLC/my. The U.S. Government is authorized to reproduce and distribute reprints for government purposes notwithstanding any copyright notation herein. The views and conclusions contained herein are those of the authors and should not be interpreted as necessarily representing the official policies or endorsements, either expressed or implied, of the Army Research Laboratory (ARL) or the U.S. Government.

Disclosures. The authors declare no conflicts of interest.

REFERENCES

1. G. Moody, V. J. Sorger, D. J. Blumenthal, P. W. Juodawlkis, W. Loh, C. Sorace-Agaskar, A. E. Jones, K. C. Balram, J. C. Matthews, A. Laing *et al.*, J. Physics: Photonics **4**, 012501 (2022).
2. R. J. Niffenegger, J. Stuart, C. Sorace-Agaskar, D. Kharas, S. Bramhavar, C. D. Bruzewicz, W. Loh, R. T. Maxson, R. McConnell, D. Reens *et al.*, Nature **586**, 538 (2020).
3. A. D. Ludlow, M. M. Boyd, J. Ye, E. Peik, and P. O. Schmidt, Rev. Mod. Phys. **87**, 637 (2015).
4. M. Soltani, R. Soref, T. Palacios, and D. Englund, Opt. express **24**, 25415 (2016).
5. D. J. Wineland, R. E. Drullinger, and F. L. Walls, Phys. Rev. Lett. **40**, 1639 (1978).
6. H. J. Metcalf and P. van der Straten, JOSA B **20**, 887 (2003).
7. D. Kielpinski, M. Cetina, J. Cox, and F. X. Kaertner, Opt. letters **31**, 757 (2006).
8. L. J. Mullen, A. J. Vieira, P. Herezfeld, and V. M. Contarino, IEEE Transactions on microwave theory techniques **43**, 2370 (1995).
9. M. Chi, O. B. Jensen, A. K. Hansen, P. M. Petersen, and Y. Ma, Laser Technol. Its Appl. pp. 3–21 (2019).
10. A. S. Raja, A. S. Voloshin, H. Guo, S. E. Agafonova, J. Liu, A. S. Gorodnitskiy, M. Karpov, N. G. Pavlov, E. Lucas, R. R. Galiev *et al.*, Nat. communications **10**, 1 (2019).
11. G. Lihachev, J. Riemensberger, W. Weng, J. Liu, H. Tian, A. Siddharth, V. Snigirev, V. Shadymov, A. Voloshin, R. N. Wang *et al.*, Nat. communications **13**, 3522 (2022).
12. M. Corato-Zanarella, A. Gil-Molina, X. Ji, M. C. Shin, A. Mohanty, and M. Lipson, Nat. Photonics pp. 1–8 (2022).
13. A. Yariv, IEEE Photonics Technol. Lett. **14**, 483 (2002).
14. A. A. Savchenkov, S.-W. Chiow, M. Ghasemkhani, S. Williams, N. Yu, R. C. Stirbl, and A. B. Matsko, Opt. letters **44**, 4175 (2019).
15. T.-J. Lu, M. Fanto, H. Choi, P. Thomas, J. Steidle, S. Mouradian, W. Kong, D. Zhu, H. Moon, K. Berggren *et al.*, Opt. express **26**, 11147 (2018).
16. X. Liu, A. W. Bruch, Z. Gong, J. Lu, J. B. Surya, L. Zhang, J. Wang, J. Yan, and H. X. Tang, Optica **5**, 1279 (2018).
17. G. N. West, W. Loh, D. Kharas, C. Sorace-Agaskar, K. K. Mehta, J. Sage, J. Chiaverini, and R. J. Ram, Apl Photonics **4**, 026101 (2019).
18. T. J. Morin, L. Chang, W. Jin, C. Li, J. Guo, H. Park, M. A. Tran, T. Komljenovic, and J. E. Bowers, Optica **8**, 755 (2021).
19. A. Siddharth, T. Wunderer, G. Lihachev, A. S. Voloshin, C. Haller, R. N. Wang, M. Teepe, Z. Yang, J. Liu, J. Riemensberger *et al.*, APL Photonics **7**, 046108 (2022).
20. G. Di Domenico, S. Schilt, and P. Thomann, Appl. optics **49**, 4801 (2010).